Single Image Super-Resolution via Iterative Collaborative Representation

Yulun Zhang[1(✉)], Yongbing Zhang[1], Jian Zhang[2], Haoqian Wang[1], and Qionghai Dai[1,3]

[1] Graduate School at Shenzhen, Tsinghua University, Shenzhen 518055, China
zhangy114@mails.tsinghua.edu.cn
[2] Institute of Digital Media, Peking University, Beijing 100871, China
[3] Department of Automation, Tsinghua University, Beijing 100084, China

Abstract. We propose a new model called iterative collaborative representation (ICR) for image super-resolution (SR). Most of popular SR approaches extract low-resolution (LR) features from the given LR image directly to recover its corresponding high-resolution (HR) features. However, they neglect to utilize the reconstructed HR image for further image SR enhancement. Based on this observation, we extract features from the reconstructed HR image to progressively upscale LR image in an iterative way. In the learning phase, we use the reconstructed and the original HR images as inputs to train the mapping models. These mapping models are then used to upscale the original LR images. In the reconstruction phase, mapping models and LR features extracted from the LR and reconstructed image are then used to conduct image SR in each iteration. Experimental results on standard images demonstrate that our ICR obtains state-of-the-art SR performance quantitatively and visually, surpassing recently published leading SR methods.

Keywords: Iterative collaborative representation · Super-resolution

1 Introduction

Single image super-resolution (SR), a classical and important problem in image processing and computer vision, aims at restoring a high-resolution (HR) image from its degraded low-resolution (LR) measurement, while minimizing visual artifacts as far as possible. Recent popular and state-of-the-art SR methods are mostly based on machine learning (ML). These methods either establish the mapping relationships between the LR and HR features from external low- and high-resolution exemplar pairs [1,2,4,6,8,9,12,14,15,17], or learn an end-to-end mapping between the LR and HR images by a deep learning technique [3]. These methods have been obtaining superior and challenging results, but neglect to use the reconstructed image for further SR enhancement.

This work was partially supported by the National Natural Science Foundation of China under Grant 61170195, U1201255, and U1301257.

Y.-S. Ho et al. (Eds.): PCM 2015, Part II, LNCS 9315, pp. 63–73, 2015.
DOI: 10.1007/978-3-319-24078-7_7

The neighbor embedding (NE) based [1,2] and sparse coding (SC) based methods [8,9,14,15] are the main streams and represent the state-of-the-art methods among the ML-based algorithms. These methods often upscale the LR input to the size of the desired HR image using simple interpolation-based methods (e.g., Bicubic interpolation) as a start of SR. In these methods, great efforts have been taken to extract features from the up-scaled LR images and learn the mapping relationships between the features of LR and HR images. Similar to Zeyde's method in [15] LR features are extracted to recover the corresponding HR features and the overlapping reconstructed HR patches are finally averaged to obtain the desired HR images. When we apply the principal component analysis (PCA) algorithm to reduce the dimensionality of the LR features while preserving 99.9 % of the average energy, the dimensionality of the LR features would be reduced largely and far smaller than that of HR features. However, if we extract the same features as LR features above from either the reconstructed or the original HR images and apply the same PCA dimensionality reducing process, the dimensionality of the extracted features will be larger than that of LR features. This inspires us to make an assumption that the reconstructed HR image contains more useful information than the interpolated LR image for high-quality image SR. So, why not utilize the reconstructed HR image as an intermediary result for the final HR image reconstruction?

Motivated by the observation above, in this paper, we propose a simple yet efficient model called iterative collaborative representation (ICR). We make use of the reconstructed HR image as an intermediary result for further image SR in an iterative way. The main difference between our method and the popular

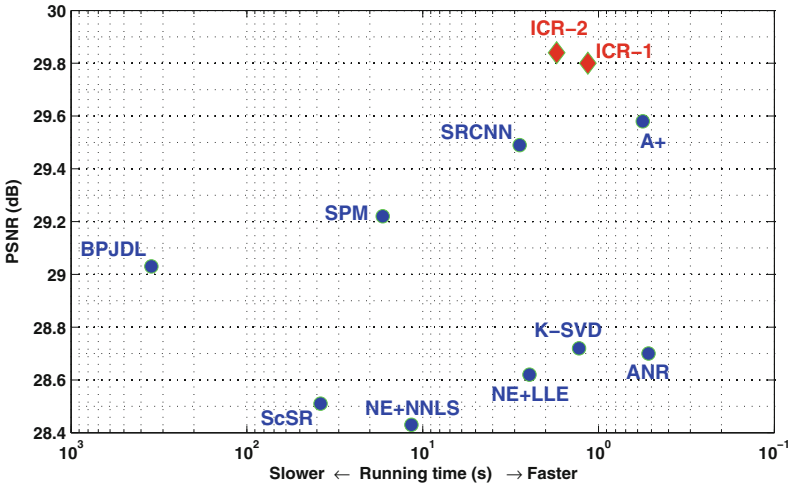

Fig. 1. Average running time (s) versus PSNR (dB) for the tested super-resolution (SR) methods (scaling factor $s = 3$). The proposed ICR (shown in red) obtains the state-of-the-art SR results and maintains competitive speed in comparison to other ML-based methods. More details are shown in Tables 1 and 2 (Color figure online).

ML-based approaches [1–4,6,8,9,12,14,15,17] lies in that we extract LR features from the reconstructed HR image to recover the next better reconstructed HR image. Based on Timofte *et al.*'s work about using collaborative representation [16] for fast image SR [8,9], we learn the projection matrices mapping LR feature spaces to HR feature spaces offline for each iteration in the learning phase. The goal is to further improve the final HR output in an iterative way. As a result, our ICR achieves superior high-quality results compared with the previous most efficient SR methods, such as SRCNN [3] and A+ [9], while maintaining computation efficiency (see Fig. 1) without additional enhancement processes, like back-projection method [5] in Yang *et al.*'s [14] and He *et al.*'s [4] work.

Overall, the contributions of this work can be mainly summarized as follows. **First**, we assume that the reconstructed HR image contains more useful information than that of the original interpolated image generated by simple methods (e.g., Bicubic interpolation). We extract LR features from the reconstructed HR image for further image SR. **Second**, we present an iterative collaborative representation model for image SR. The model would enhance the quality of the SR results significantly by only one iteration. **Third**, we demonstrate that ICR is useful in SR and can achieve high-quality and speed efficiently with little pre/post-processing.

2 Related Work

Neighbor embedding (NE) [1,2], sparse coding (SC) [4,6,8,9,14,15], and deep learning [3] approaches are the three main types of ML-based SR algorithms, which train the mapping relationships between LR and HR features. Chang *et al.* [2] generated HR patches by using a manifold embedding technique. Bevilacqua *et al.* [1] proposed another NE-based SR algorithm using nonnegative neighbor embedding. Yang *et al.* [13,14] proposed a SC-based SR algorithm by assuming that LR and HR features share the same reconstruction coefficients over their corresponding LR and HR dictionaries. This work was further developed by Zeyde *et al.* [15], who utilized PCA and orthogonal matching pursuit (OMP) [10] to reduce the dimensionality of LR features and solve sparse representation respectively. More sophisticated SC formulations were proposed recently, for example, a Bayesian method using a beta process prior was applied to learn the over-complete dictionaries in [4] and a statistical prediction model based on sparse representation was used in [6]. At the same time, fast SR algorithms were proposed by combining dictionary learning [8] or clustering [12] and regression. Timofte *et al.* proposed anchored neighborhood regression (ANR) [8] learning sparse dictionaries and regressors anchored to the dictionary atoms. Yang *et al.* proposed to cluster features into numerous subspaces and created simple mapping functions to generate SR images [12]. Very recently, Dong *et al.* [3] proposed a model super-resolution convolutional neural network (SRCNN) by using a deep learning method. In these methods, the SR procedure started by interpolating the LR input to the size of the desired HR image and did not utilize the reconstructed HR image for further image SR.

Collaborative representation mainly developed by Zhang *et al.* has recently shown an extensive popularity partially due to its powerful performance in pattern classification [16]. By combining dictionary learning and collaborative representation [16], Timofte *et al.* proposed adjusted anchored neighborhood regression (A+) [9] by learning the regressors from the full training material. This work was further improved in [17] by Zhang *et al.*, who employed unified mutual coherence between the dictionary atoms and atoms/samples when training the dictionary and sampling anchored neighbors for image SR. These methods obtained state-of-the-art SR results with fast speed by introducing collaborative representation [16], from which our ICR also benefits.

Based on the fact that there have been a few studies of using the reconstructed image for further SR, we propose the ICR model. In this model, we study the mapping relationships between features of the reconstructed HR image and its corresponding original HR image. The major steps of our ICR are illustrated in Fig. 2. To the best of our knowledge, the image SR problem has not witnessed such an SR framework.

3 Iterative Collaborative Representation for Super-Resolution

3.1 Image SR Based on Collaborative Representation

Timofte *et al.* proposed ANR [8] and A+ [9] for fast image SR by using collaborative representation [16]. Based on these works, we give a brief review of the pipeline of collaborative representation [16] based SR. Let $\left\{\boldsymbol{y}_L^i\right\}_{i=1}^{N_s}$ and $\left\{\boldsymbol{y}_H^i\right\}_{i=1}^{N_s}$ be the LR and HR features set extracted from LR/HR training images, the dimensionality of these LR features have been reduced by a PCA projection matrix $\mathbf{P}$. Then the LR dictionary $\boldsymbol{D} = \{\boldsymbol{d}_k\}_{k=1}^{K}$ is trained in the LR feature space. For each LR dictionary atom $\boldsymbol{d}_k$, we group its LR anchored neighborhood $\boldsymbol{N}_{L,k}$ by searching max nearest training LR features and the corresponding HR features are used to form $\boldsymbol{N}_{H,k}$. We use collaborative representation [16] with l_2-norm regularized least squares regression to obtain the projection matrix for each LR-HR feature neighborhood $\{\boldsymbol{N}_{L,k}, \boldsymbol{N}_{H,k}\}_{k=1}^{K}$. The problem becomes

$$\boldsymbol{x}_i = arg\ \min_{\boldsymbol{x}_i} \left\|\boldsymbol{y}_L^i - \boldsymbol{N}_{L,k} \cdot \boldsymbol{x}_i\right\|_2^2 + \lambda \left\|\boldsymbol{x}_i\right\|_2^2, \tag{1}$$

where $\boldsymbol{y}_L^i \in \mathbb{R}^{n\times 1}$ is an arbitrary LR feature, $\boldsymbol{N}_{L,k}$ is the LR neighborhood whose corresponding LR dictionary atom $\boldsymbol{d}_k$ is the closet to $\boldsymbol{y}_L^i$, $\boldsymbol{x}_i$ is the coefficient vector of $\boldsymbol{y}_L^i$ over $\boldsymbol{N}_{L,k}$, and $\lambda > 0$ is a weighting parameter. The problem above has a closed-form solution given by

$$\boldsymbol{x}_i = \left(\boldsymbol{N}_{L,k}^T \boldsymbol{N}_{L,k} + \lambda \boldsymbol{I}\right)^{-1} \boldsymbol{N}_{L,k}^T \boldsymbol{y}_L^i, \tag{2}$$

from which we can compute the corresponding projection matrix $\boldsymbol{F}_k$ offline by

$$\boldsymbol{F}_k = \boldsymbol{N}_{H,k} \left(\boldsymbol{N}_{L,k}^T \boldsymbol{N}_{L,k} + \lambda \boldsymbol{I}\right)^{-1} \boldsymbol{N}_{L,k}^T, \quad k = 1, ..., K. \tag{3}$$

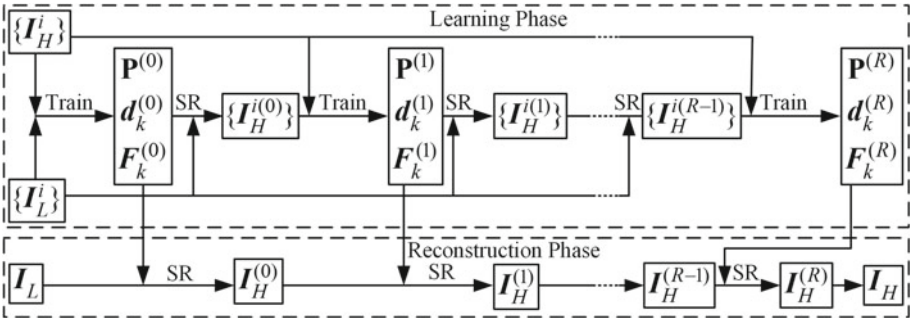

Fig. 2. Pipeline of our iterative collaborative representation framework.

The SR problem can then be solved by calculating for each LR feature $\boldsymbol{y}_L^i$ its nearest dictionary atom $\boldsymbol{d}_k$, followed by converting $\boldsymbol{y}_L^i$ to its HR feature $\boldsymbol{y}_H^i$ with the stored projection matix $\boldsymbol{F}_k$ via

$$\boldsymbol{y}_H^i = \boldsymbol{F}_k \boldsymbol{y}_L^i. \tag{4}$$

3.2 Learning Phase in ICR

As shown in Fig. 2, the original LR and HR training images are used to obtain the PCA transform matrix $\mathbf{P}^{(0)}$, LR dictionary atoms $\left\{\boldsymbol{d}_k^{(0)}\right\}_{k=1}^{K}$, and their corresponding projection matrices $\left\{\boldsymbol{F}_k^{(0)}\right\}_{k=1}^{K}$ mapping LR feature $\boldsymbol{y}_L$ to its corresponding HR feature $\boldsymbol{y}_H$. Here, we utilize the same process as that in A+ [9] for the following three reasons: First, the LR features are first- and second-order gradients in the horizontal and vertical directions from the interpolated LR images, as a result, this type of features will be sensitive to the region whose gradients change obviously. Second, the SR results obtained by A+ [9] usually have sharper edges and less artifacts (e.g., ringing artifacts) along the edges than that of most of other state-of-the-art methods (see Figs. 4, 5, 6, and 7). Third, by using one of the published most efficient SR methods as a start point for our implementation, we can demonstrate the effectiveness of our proposed ICR model clearly.

We then utilize A+ [9] to upscale the original LR training images $\left\{\boldsymbol{I}_L^i\right\}_{i=1}^{N_I}$ to $\left\{\boldsymbol{I}_H^{i(0)}\right\}_{1=1}^{N_I}$, whose size is the same as that of their original HR images $\left\{\boldsymbol{I}_H^i\right\}_{i=1}^{N_I}$. In our ICR model, we regard $\left\{\boldsymbol{I}_H^{i(r-1)}\right\}_{r=1}^{R}$ (R is the total number of iteration) as LR images for simplicity. In the r-th iteration of the learning phase, we extract LR and HR feature pairs from $\left\{\boldsymbol{I}_H^{i(r-1)}, \boldsymbol{I}_H^i\right\}_{i=1}^{N_I}$ to learn PCA transform matrix $\mathbf{P}^{(r)}$, LR dictionary atoms $\left\{\boldsymbol{d}_k^{(r)}\right\}_{k=1}^{K}$, and projection matrices $\left\{\boldsymbol{F}_k^{(r)}\right\}_{k=1}^{K}$ using

the similar training pipeline as A+ [9] with a little difference. Different from A+ [9] using the Euclidean distance between the dictionary atoms and the training samples when anchored neighborhoods are grouped, we utilize the mutual coherence $\boldsymbol{c}_{k,i}$ between $\boldsymbol{d}_k^{(r)}$ and $\boldsymbol{y}_L^i$ via

$$\boldsymbol{c}_{k,i} = \left| [\boldsymbol{d}_k^{(r)}]^{\mathrm{T}} \boldsymbol{y}_L^i \right|, \tag{5}$$

where $\boldsymbol{d}_k^{(r)}$ is k-th atom in the learned dictionary $\boldsymbol{D}^{(r)} = \left\{ \boldsymbol{d}_k^{(r)} \right\}_{k=1}^{K}$ and $\boldsymbol{y}_L^i$ is an LR training sample. By using the mutual coherence $\boldsymbol{c}_{k,i}$, we not only comply with distance measurements between LR features and dictionary atoms in the reconstruction phase, but also speed up about 25 % in computational time compared with that in A+ [9].

3.3 Reconstruction Phase in ICR

As we learned R relationship projecting models $\left\{ \mathbf{P}^{(r)}, \left\{ \boldsymbol{d}_k^{(r)}, \boldsymbol{F}_k^{(r)} \right\}_{k=1}^{K} \right\}_{r=1}^{R}$ after R iterations in the learning phase, the SR problem can then be efficiently solved in an iterative way (see the reconstruction phase in Fig. 2). For an LR input image $\boldsymbol{I}_L$, we upscale it to $\boldsymbol{I}_H^{(0)}$ by A+ [9] as the initial input for our ICR model. In the r-th iteration of the reconstruction phase, we extract a set of LR features $\left\{ \boldsymbol{y}_L^{i(r-1)} \right\}$ from the reconstructed HR image $\boldsymbol{I}_H^{(r-1)}$. For each LR feature $\boldsymbol{y}_L^{i(r-1)}$, we search its nearest atom $\boldsymbol{d}_k^{(r)}$ with highest coherence $c_{k,i}$ from the LR dictionary $\boldsymbol{D}^{(r)}$, followed by recovering its HR feature $\boldsymbol{y}_H^{i(r)}$ via (4). The HR patch $\boldsymbol{p}_H^{i(r)}$ is then obtained by adding HR feature $\boldsymbol{y}_H^{i(r)}$ to the corresponding interpolated LR patch $\boldsymbol{p}_L^i$ and we combine these HR patches to a whole HR image $\boldsymbol{I}_H^{(r)}$ by averaging the intensity values over the overlapping regions. Finally, we obtain the R-th SR result $\boldsymbol{I}_H^{(R)}$ as our final HR output $\boldsymbol{I}_H$.

4 Experimental Results

In this section, a series of experiments are reported to demonstrate the efficiency and robustness of our proposed ICR-based SR algorithm compared with other state-of-the-art methods.

Fig. 3. 8 test images from left to righ: bike, bird, butterfly, flowers, plants, ppt3, starfish, and woman.

4.1 Experimental Settings

In our experiments, for a fair comparison, we use 91 training images proposed by Yang *et al.* [13]. The experiment is conducted on 8 commonly used LR natural images shown in Fig. 3, including humans, animals, and plants. Peak signal-to-noise ratio (PSNR), structural similarity (SSIM) [11], and visual information fidelity (VIF) [7] are employed in our experiments to evaluate the quality of the SR results. All of these evaluation metrics are performed between the luminance channel of the original HR and the reconstructed image. We compare our ICR with Bicubic interpolation and 9 state-of-the-art ML-based SR methods: NE+LLE [2], ScSR [14], K-SVD [15], NE+NNLS [1], ANR [8], BPJDL [4], SPM [6], SRCNN [3], and A+ [9]. The implementations are all from the publicly available codes provided by the authors[1].

We down-sample the original HR images to generate LR images for training and testing on the luminance channel by Bicubic interpolation. We set scaling factor $s = 3$ and the total number of iteration $R = 2$ throughout the paper. Same as A+[9], we set $K = 1024, max = 2048, \lambda = 0.1$ in a set of experimental results.

4.2 Performance

We compare the proposed ICR with other state-of-the-art methods in terms of PSNR, SSIM, and VIF values in Table 1, where the results of ICR-1 and ICR-2 are produced by our ICR model. $R = 1$ and $R = 2$ are set in ICR-1 and ICR-2 respectively. Although ICR does not outperform all of the competing methods for each test image, ICR obtains best results on average in terms of PSNR. On the other hand, ICR achieves the best results for each image in terms of SSIM and VIF. This demonstrates that ICR recovers more structural details than other methods. According to Table 1, a large average PSNR, SSIM, and VIF gains of our ICR-2 over the second best method A+ [9] (regardless of ICR-1) are 0.26 dB, 0.007, and 0.017. Such an improvement is notable, since A+ [9] has been the most efficient dictionary-based SR method so far. This indicates that our ICR is efficient for high-quality image SR by using features extracted from the reconstructed HR image in each iteration. Another amazing phenomenon is that even we conduct only one iteration (i.e., $R = 1$), the SR results by ICR-1 can also outperform the second best method A+ [9] by a large average PSNR, SSIM, and VIF gains. While, the average PSNR, SSIM, and VIF gains of ICR-2 over ICR-1 is very smal. As a result, $R = 1$ or $R = 2$ is an optimal value to balance the quality of SR and computation complexity.

Table 2 shows the running time comparisons of numerous methods with a scaling factor $s = 3$ in the SR phase. We profile the running time of all the methods in a MATLAB 2012a environment using the same machine (3.20 GHz Core(TM) i5-3470 with 16 GB RAM). According to Table 2, ICR ranks the third or fourth place with a very small gap between ICR and the fastest method ANR. And one iteration in our ICR would take very little time while enhancing the SR results significantly.

[1] The source code of the proposed ICR will be available after this paper is published.

Table 1. Quantitative comparisons on PSNR (dB), SSIM, and VIF for 3× magnification. For each image, there are three rows: PSNR (dB), SSIM, and VIF. The best result for each image is highlighted.

Images	BI	NE+LLE [2]	ScSR [14]	K-SVD [15]	NE+NNLS [1]	ANR [8]	BPJDL [4]	SPM [6]	SRCNN [3]	A+ [9]	ICR-1	ICR-2
bike	22.83	23.89	23.97	23.89	23.76	23.98	24.23	24.45	24.51	24.68	24.85	**24.92**
	0.704	0.765	0.767	0.765	0.756	0.769	0.781	0.788	0.787	0.798	0.805	**0.808**
	0.310	0.383	0.354	0.382	0.371	0.389	0.404	0.409	0.397	0.422	0.434	**0.437**
bird	32.63	34.54	34.20	34.62	34.16	34.63	34.88	35.15	34.97	35.60	**35.79**	35.68
	0.926	0.948	0.940	0.948	0.943	0.949	0.950	0.952	0.950	0.956	0.958	**0.959**
	0.552	0.659	0.587	0.657	0.640	0.665	0.675	0.668	0.658	0.692	0.704	**0.706**
butter-fly	24.04	25.73	25.69	25.99	25.45	25.89	26.52	26.78	27.59	27.34	27.53	**27.63**
	0.822	0.868	0.862	0.877	0.861	0.870	0.887	0.899	0.901	0.910	0.915	**0.917**
	0.365	0.459	0.416	0.467	0.446	0.468	0.500	0.507	0.516	0.532	0.545	**0.551**
flowers	27.28	28.42	28.33	28.48	28.23	28.52	28.78	28.86	29.02	29.10	29.29	**29.34**
	0.803	0.839	0.831	0.839	0.832	0.841	0.847	0.847	0.849	0.854	0.858	**0.859**
	0.370	0.448	0.401	0.448	0.436	0.453	0.468	0.464	0.462	0.481	0.491	**0.495**
plants	31.30	32.81	32.52	32.79	32.63	32.81	33.13	33.14	33.52	33.79	34.07	**34.16**
	0.872	0.905	0.894	0.904	0.900	0.905	0.910	0.907	0.911	0.921	0.926	**0.927**
	0.476	0.590	0.514	0.582	0.574	0.593	0.605	0.590	0.599	0.634	0.648	**0.655**
ppt3	23.90	25.20	25.32	25.49	25.20	25.28	25.55	25.87	26.32	26.36	26.61	**26.67**
	0.884	0.912	0.908	0.920	0.910	0.913	0.921	0.926	0.929	0.939	0.944	**0.945**
	0.371	0.448	0.420	0.462	0.444	0.452	0.473	0.481	0.482	0.521	0.540	**0.547**
star-fish	27.01	28.15	28.04	28.14	28.04	28.18	28.46	28.79	**29.04**	28.63	28.83	28.88
	0.814	0.852	0.846	0.851	0.847	0.853	0.860	0.865	0.871	0.864	0.870	**0.872**
	0.373	0.447	0.397	0.446	0.438	0.451	0.464	0.470	0.471	0.473	0.483	**0.486**
woman	28.57	30.21	29.99	30.36	30.01	30.30	30.73	30.69	30.92	31.18	31.41	**31.45**
	0.890	0.916	0.904	0.917	0.912	0.917	0.921	0.923	0.924	0.929	0.931	**0.932**
	0.454	0.559	0.481	0.562	0.549	0.562	0.580	0.579	0.571	0.605	0.617	**0.622**
Aver-age	27.19	28.62	28.51	28.72	28.43	28.70	29.03	29.22	29.49	29.58	29.80	**29.84**
	0.839	0.876	0.869	0.878	0.870	0.877	0.885	0.888	0.890	0.896	0.901	**0.903**
	0.409	0.499	0.446	0.501	0.487	0.504	0.521	0.521	0.520	0.545	0.558	**0.562**

Table 2. Running time (seconds) comparisons of different methods

Methods	NE+LLE [2]	ScSR [14]	K-SVD [15]	NE+NNLS [1]	ANR [8]	BPJDL [4]	SPM [6]	SRCNN [3]	A+ [9]	ICR-1	ICR-2
Time	2.47	38.12	1.29	11.59	0.52	349.13	16.88	2.81	0.56	1.15	1.73

4.3 Visual Results

To further demonstrate the effectiveness of ICR, in Figs. 4, 5, 6, and 7 we compare our visual results with that of ANR, BPJDL, SPM, SRCNN, and A+, as they perform the best among all existing methods. As we can see from Figs. 4 and 6, ANR, BPJDL, SPM, and SRCNN would always produce obvious ringing artifacts along the edges and fail to recover detailed textures. A+ can alleviate the blurring and ringing artifacts along the main edges, however, it also generates blurred edges (see Fig. 5) and introduces some unpleasing artifacts (see Fig. 7) when compared to ICR. This also helps to demonstrate that the reconstructed HR image contains more useful information than the interpolated LR image for better SR performance. As can be observed, our ICR produces sharper edges without obvious ringing effects (see Figs. 4 and 7), less blurring effects (see Fig. 5), and finer textures with more details (see Fig. 6).

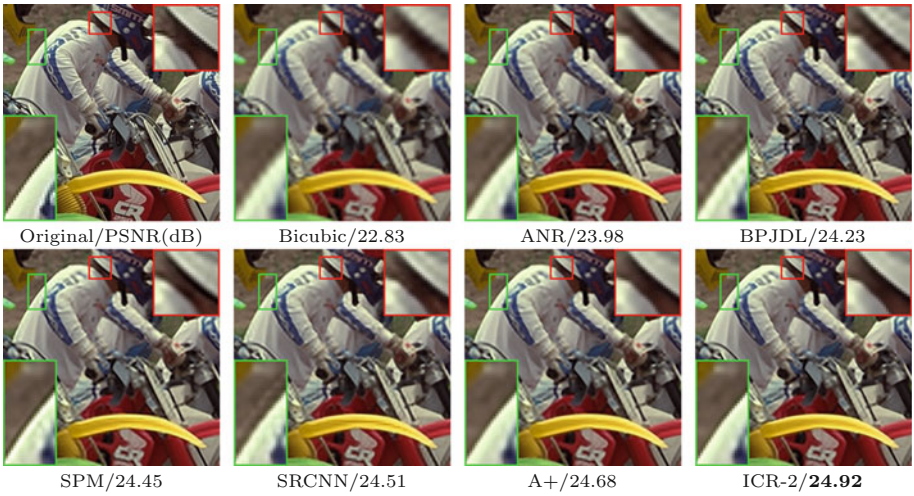

Fig. 4. Visual comparisons on **bike** with a scaling factor 3.

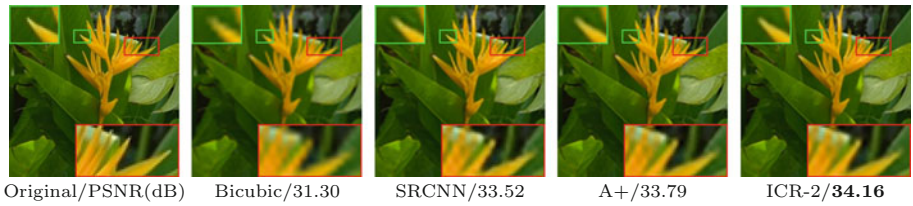

Fig. 5. Visual comparisons on **plants** with a scaling factor 3.

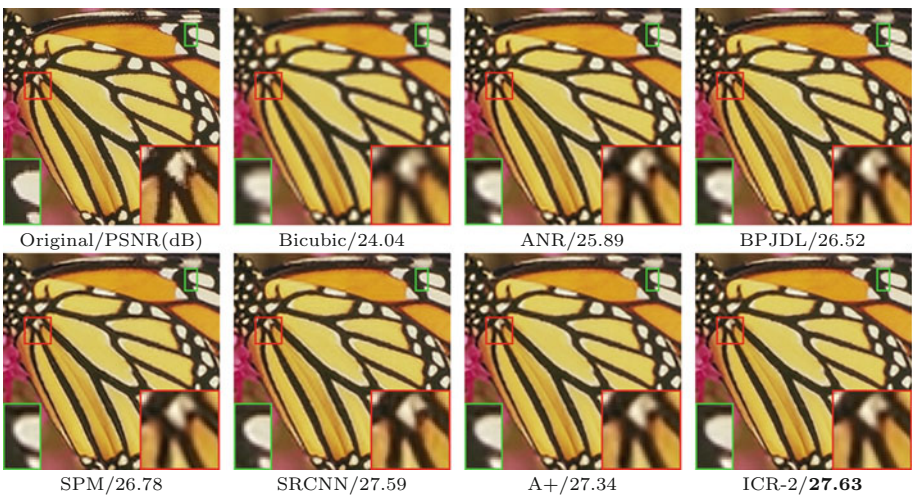

Fig. 6. Visual comparisons on **butterfly** with a scaling factor 3.

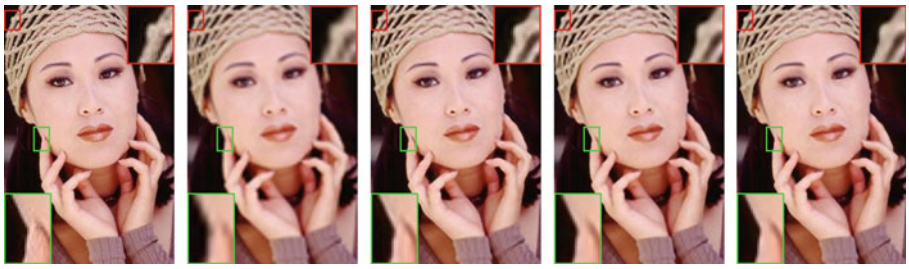

Fig. 7. Visual comparisons on **woman** with a scaling factor 3.

5 Conclusion

In this paper, we proposed a simple yet efficient image SR method. We assume that more useful information is contained in the reconstructed HR image, from which we extract LR features for further image SR. Our ICR model employs dictionary learning and collaborative representation [16] to learn numerous projection matrices offline in each iteration. By using these projection matrices, we first upscale the LR image to obtain the initial HR image, from which we extract LR features to reconstruct the next better HR image. When compared with other state-of-the-art methods, our ICR shows the best performance both in terms of objective evaluation metrics and subjective visual results. We conjecture that additional performance can be gained by using more iterations and different feature extraction strategies.

References

1. Bevilacqua, M., Roumy, A., Guillemot, C., Alberi-Morel, M.L.: Low-complexity single-image super-resolution based on nonnegative neighbor embedding. In: BMVC (Sep 2012)
2. Chang, H., Yeung, D.Y., Xiong, Y.: Super-resolution through neighbor embedding. In: CVPR, pp. 1–6 (2004)
3. Dong, C., Loy, C.C., He, K., Tang, X.: Learning a deep convolutional network for image super-resolution. In: Fleet, D., Pajdla, T., Schiele, B., Tuytelaars, T. (eds.) ECCV 2014, Part IV. LNCS, vol. 8692, pp. 184–199. Springer, Heidelberg (2014)
4. He, L., Qi, H., Zaretzki, R.: Beta process joint dictionary learning for coupled feature spaces with application to single image super-resolution. In: CVPR, pp. 345–352 (2013)
5. Irani, M., Peleg, S.: Motion analysis for image enhancement: Resolution, occlusion, and transparency. J. Vis. Commun. Image Represent. **4**(4), 324–335 (1993)
6. Peleg, T., Elad, M.: A statistical prediction model based on sparse representations for single image super-resolution. IEEE Trans. Image Process. **23**(6), 2569–2582 (2014)
7. Sheikh, H.R., Bovik, A.C.: Image information and visual quality. IEEE Trans. Image Process. **15**(2), 430–444 (2006)

8. Timofte, R., De, V., Gool, L.V.: Anchored neighborhood regression for fast example-based super-resolution. In: ICCV, pp. 1920–1927 (2013)
9. Timofte, R., De Smet, V., Van Gool, L.: A+: adjusted anchored neighborhood regression for fast super-resolution. In: Cremers, D., Reid, I., Saito, H., Yang, M.-H. (eds.) ACCV 2014. LNCS, vol. 9006, pp. 111–126. Springer, Heidelberg (2015)
10. Tropp, J.A., Gilbert, A.C.: Signal recovery from random measurements via orthogonal matching pursuit. IEEE Trans. Inf. Theor. **53**(12), 4655–4666 (2007)
11. Wang, Z., Bovik, A.C., Sheikh, H.R., Simoncelli, E.P.: Image quality assessment: from error visibility to structural similarity. IEEE Trans. Image Process. **13**(4), 600–612 (2004)
12. Yang, C.Y., Yang, M.H.: Fast direct super-resolution by simple functions. In: ICCV, pp. 561–568 (2013)
13. Yang, J., Wright, J., Huang, T., Ma, Y.: Image super-resolution as sparse representation of raw image patches. In: CVPR, pp. 1–8 (2008)
14. Yang, J., Wright, J., Huang, T.S., Ma, Y.: Image super-resolution via sparse representation. IEEE Trans. Image Process. **19**(11), 2861–2873 (2010)
15. Zeyde, R., Elad, M., Protter, M.: On single image scale-up using sparse-representations. In: Proceedings of the 7th International Conference Curves Surfing, pp. 711–730 (2010)
16. Zhang, L., Yang, M., Feng, X.: Sparse representation or collaborative representation: Which helps face recognition? In: ICCV, pp. 471–478 (2011)
17. Zhang, Y., Gu, K., Zhang, Y., Zhang, J., Dai, Q.: Image super-resolution based on dictionary learning and anchored neighborhood regression with mutual incoherence. In: ICIP (2015)